Criticality in the Approach to Failure in Amorphous Solids

Jie Lin,[1,*] Thomas Gueudré,[2] Alberto Rosso,[3] and Matthieu Wyart[4]
[1]Center for Soft Matter Research, Department of Physics, New York University, New York, New York 10003, USA
[2]DISAT, Politecnico Corso Duca degli Abruzzi, I-10129 Torino, Italy
[3]Laboratoire de Physique Théorique et Modèles Statistiques (UMR CNRS 8626), Université de Paris–Sud, Orsay Cedex 91405, France
[4]Institute of Theoretical Physics, Ecole Polytechnique Federale de Lausanne (EPFL), CH-1015 Lausanne, Switzerland
(Received 12 May 2015; published 16 October 2015)

Failure of amorphous solids is fundamental to various phenomena, including landslides and earthquakes. Recent experiments indicate that highly plastic regions form elongated structures that are especially apparent near the maximal shear stress $\Sigma_{\max}$ where failure occurs. This observation suggested that $\Sigma_{\max}$ acts as a critical point where the length scale of those structures diverges, possibly causing macroscopic transient shear bands. Here, we argue instead that the entire solid phase ($\Sigma < \Sigma_{\max}$) is critical, that plasticity always involves system-spanning events, and that their magnitude diverges at $\Sigma_{\max}$ independently of the presence of shear bands. We relate the statistics and fractal properties of these rearrangements to an exponent θ that captures the stability of the material, which is observed to vary continuously with stress, and we confirm our predictions in elastoplastic models.

DOI: 10.1103/PhysRevLett.115.168001 PACS numbers: 45.70.-n, 63.50.-x, 64.60.av

Amorphous solids, such as emulsions, sand, and molecular glasses, are yield stress materials: they behave as solids if the applied shear stress Σ is low, but they flow as fluids if it is large. Unlike the melting transition, the associated phase transition is dynamical: the solid phase is an arrested, glassy state whose properties depend on preparation. One such property is failure [1], which occurs as Σ increases toward a history-dependent stress $\Sigma_{\max}$ where macroscopic flow starts. For densely prepared materials, the stress overshoots: $\Sigma_{\max} > \Sigma_c$ [2,3], where Σ_c is the minimum stress at which flow can be maintained in stationary conditions. Flow then tends to localize along transient (but sometimes long lasting) shear bands [4]. By contrast, for loosely prepared materials, $\Sigma_{\max} = \Sigma_c$ [2] and shear banding may be avoided [5]. Despite its importance in human applications and geophysical phenomena, including landslides and earthquakes [6], the microscopic mechanisms controlling plasticity and failure remain in debate.

In granular materials, recent experiments [7–9] and numerics [10] support that, for $\Sigma < \Sigma_{\max}$, plasticity occurs via localized rearrangements, or shear transformations [11], which tend to organize into elongated structures whose magnitude grows as $\Sigma \to \Sigma_{\max}$. In Ref. [10] it was argued that for a dense initial state ($\Sigma_{\max} > \Sigma_c$), $\Sigma_{\max}$ acts as a critical point where a correlation length ξ diverges and avalanches become system spanning, which may in turn trigger macroscopic shear bands. This viewpoint complements the growing consensus that the reverse transition, occurring when flows stop as the stress is decreased toward Σ_c, is accompanied by a diverging length scale [12–18]. Such a "symmetric" scenario, where ξ diverges from both sides of the transition, applies to the depinning transition [19] of an elastic manifold pushed through a disordered medium. Nevertheless, an alternative scenario has been argued for in glassy systems with slowly decaying interactions, predicting system-spanning avalanches ($\xi = \infty$) in the entire glass phase [20]. Applied to amorphous solids, this view suggests criticality for all stresses $\Sigma < \Sigma_{\max}$ where plasticity occurs. This approach, however, lacks empirical support, and its consequences on failure near $\Sigma_{\max}$ have not been investigated.

In this Letter we show that, as the stress is adiabatically increased in the solid phase, leading to a plastic strain $\epsilon(\Sigma)$, the mean avalanche size $\langle S \rangle$ follows $\langle S \rangle \sim N^{\theta/(\theta+1)}/(\partial\Sigma/\partial\epsilon)$, where N is the system size and θ is an exponent that characterizes the stability of the structure [21]. This result confirms that avalanches are system spanning ($\xi = \infty$) for all $\Sigma < \Sigma_{\max}$, and it further implies an additional singularity as failure is approached since $\partial\Sigma/\partial\epsilon \to 0$ when $\Sigma \to \Sigma_{\max}$. We suggest that data analysis used in the literature can mistakenly interpret this singularity as a diverging length scale. We also derive a scaling relation between θ and the exponents characterizing the statistics of avalanches. We test these predictions using elastoplastic models [22,23] and show that they hold independently of the system preparation and of the presence of shear bands near $\Sigma_{\max}$, thus implying that macroscopic flow localization and singularities in avalanche size are unrelated.

Elastoplastic viewpoint.—Following Refs. [22–24], we model amorphous solids as consisting of N blocks, each characterized by a scalar local stress σ_i and a local failure threshold σ_i^{th}. The overall shear stress is $\Sigma = \sum_i \sigma_i/N$. Stability of i is achieved if $|\sigma_i| < \sigma_i^{\text{th}}$. Otherwise, the block is unstable: a plastic strain of magnitude $\Delta\epsilon_i$ occurs on some time scale τ_c, leading to an overall increment of

plastic strain $\Delta\epsilon = \Delta\epsilon_i/N$. Such a plastic event also reduces stress locally by some amount $\Delta\sigma_i = \mu\Delta\epsilon_i$, where μ is the elastic modulus, and affects stress in other locations via a long-range Eshelby field $\delta\sigma_j = G(\vec{r}_{ij})\Delta\sigma_i$ [25], which can, in turn, trigger new instabilities. For our numerics below, we choose the specific model described in Ref. [13] in two dimensions. Blocks then form a biperiodic square lattice, and the elastic propagator follows approximatively $\mathcal{G}(\vec{r}_{ij}) \propto \cos(4\phi)/r^2$, where ϕ is the angle between the shear direction and $\vec{r}_{ij}$. We choose $\sigma^{\text{th}} = \tau_c = \mu = 1$, and $\Delta\sigma_i = -\sigma_i + \delta$, where δ is a random number, uniformly distributed in $[-0.1, 0.1]$. For these choices, $\Sigma_c \simeq 0.53$, and stability is easily expressed in terms of the variable $x_i \equiv \sigma_i^{\text{th}} - \sigma_i$, and it corresponds to $x_i \in [0, 2]$.

Such automaton models can be used to study the transient regime toward failure. In what follows we use two quasistatic protocols. In the stress-control protocol, Σ is increased just sufficiently to trigger a single instability. Σ is fixed during the resulting avalanche and is increased again only when this chain of events has stopped. The strain-control protocol is identical, except that Σ decreases during avalanches, proportionally to the plastic strain. Stress- vs plastic-strain curves for these two protocols are shown in Fig. 1 (from which the stress- vs total strain γ curves are easily deduced using the relation $\Delta\gamma = \Delta\epsilon + \Delta\Sigma/\mu$). They essentially track each other macroscopically [although they differ microscopically; see the insets 1(c) and 1(d)], except when Σ reaches $\Sigma_{\max}$, if $\Sigma_{\max} > \Sigma_c$.

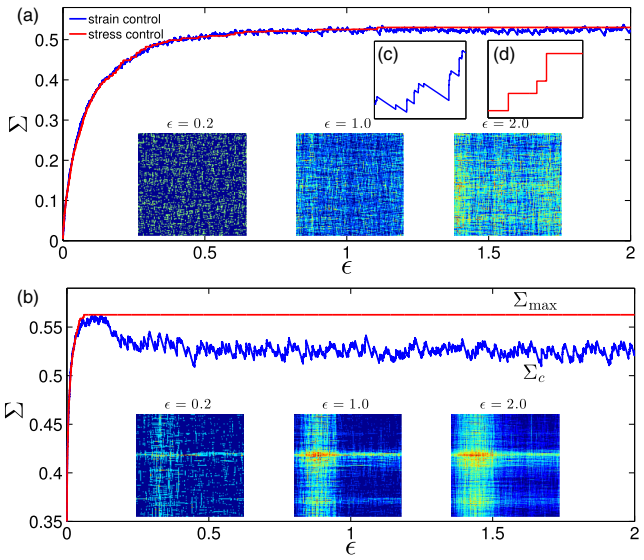

FIG. 1 (color online). Stress Σ vs plastic-strain ϵ curves for both strain- (blue) and stress-controlled (red) protocols, for (a) a broad initial distribution $P_0(x)$ and (b) a narrow $P_0(x)$. In (a) $\Sigma_{\max} = \Sigma_c$, whereas in (b) the stress overshoots and $\Sigma_{\max} > \Sigma_c$. (Insets) Spatial maps of plastic strain measured at different strain levels. Highly (weakly) plastic regions are indicated in yellow (blue). Macroscopic shear localization occur in (b) but not in (a). (c), (d) Zooming in on the stress- vs plastic-strain curves, one observes microscopic differences between the two protocols.

The transient qualitatively depends on the initial stability of the system, characterized by the initial distribution of local stability $P_0(x)$. If $P_0(x)$ is narrow and depleted near $x = 0$ (corresponding to a very stable initial condition), transient shear bands occur; otherwise, flow can remain homogeneous [26]. In Fig. 1 we confirm these results using a broad and a narrow distribution $P_0(x)$ (see the Supplemental Material [27] for details). We further find that transient shear bands tend to occur if the stress-strain curve overshoots (although we did not investigate this correlation systematically), as is sometimes reported [3,28,29] and argued for in Refs. [5,30]. In what follows we focus on an avalanche-type response, for Σ below and approaching $\Sigma_{\max}$.

Distribution of local distance to yield stress.—Mean-field models [24,31] reveal that the distribution of local stability $P(x)$ vanishes near $x = 0$ in a quasistatic shear at Σ_c. In Ref. [21] some of us showed that stability indeed requires the presence of a *pseudogap*, i.e., $P(x) \sim x^\theta$ with $\theta > 0$; otherwise, any plastic event would eventually trigger an extensive rearrangement, and this argument also holds in the transient regime. θ was measured in elasto-plastic models [21] and indirectly in MD simulations [32,33], both at Σ_c and after a quench at $\Sigma = 0$, leading to consistent results. In Fig. 2 we extend these results to the transient regime. We find that $\theta > 0$, as predicted in Ref. [21]. However, the value of θ turns out to be a function of the relative stress $\Sigma/\Sigma_{\max}$, while it converges to a well-defined value for large system size, as shown in the Supplemental Material [27]. After some initial decay at very small Σ (not shown), the value of θ increases from $\theta = 0.174 \pm 0.004$ at $\Sigma/\Sigma_{\max} \approx 0.49$ to the value $\theta = 0.6 \pm 0.004$ at $\Sigma = \Sigma_{\max}$. This measure is consistent with the exponent obtained in the stationary regime [13].

The value of $\theta(\Sigma_c)$ was argued to control rheological properties in the flowing phase as $\Sigma \to \Sigma_c$ from above [13] and to imply system-spanning avalanches for $\Sigma < \Sigma_{\max}$

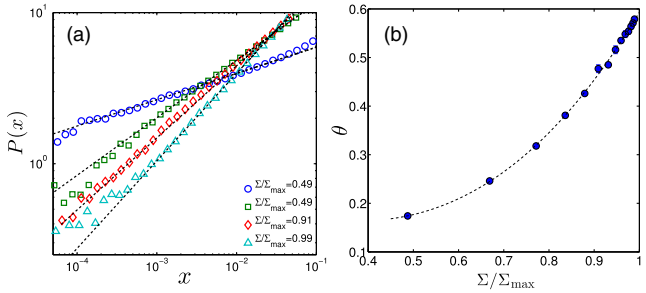

FIG. 2 (color online). (a) Distribution of local stability $P(x)$ for $\Sigma/\Sigma_{\max} = 0.49$ to 0.99 in the stress-control protocol for $N = 1024^2$ in the case $\Sigma_{\max} = \Sigma_c$. The dashed lines are direct fits of the form $P(x) \sim x^\theta$, from which we extract θ. This quantity is shown in (b). The dashed line is the interpolation using a third order polynomial fit.

[20]. We now extend this latter argument to include the case where $\Sigma \to \Sigma_{\max}$ from below.

Extreme value statistics implies that if $P(x) \sim x^{\theta}$ and the variables x_i are independent, the least stable block must be at a distance $x_{\min} \sim N^{-1/(\theta+1)}$ of an instability. By definition, $x_{\min}$ is the increment of stress that can be added before a new avalanche starts: the length of the vertical lines in Fig. 1(d). Hence, following a finite stress increment of $\Delta\Sigma$, a number $M \sim \Delta\Sigma/x_{\min} \sim \Delta\Sigma N^{1/(\theta+1)}$ of avalanches are triggered. In elastoplastic models the avalanche size S is defined as the number of plastic events, which is approximately related to the total strain of the single avalanche $\delta\epsilon$, by $S \approx N\delta\epsilon$. Thus, the total strain increase $\Delta\epsilon$ must follow $\Delta\epsilon = M\langle\delta\epsilon\rangle = M\langle S\rangle/N$, where $\langle S\rangle$ is the mean avalanche size at stress Σ. We thus get

$$\langle S\rangle = \frac{N\Delta\epsilon}{M} = \frac{N^{\theta/(1+\theta)}\Delta\epsilon}{\Delta\Sigma} \to \frac{N^{\theta/(1+\theta)}}{\partial\Sigma/\partial\epsilon}, \qquad (1)$$

where $\partial\Sigma/\partial\epsilon$ is the local slope of the stress-plastic strain curve, and the limit corresponds to $\Delta\Sigma \to 0$. This central result indicates the following. (i) If Σ is increased in the solid phase, avalanches are system spanning ($\xi = \infty$) even for $\Sigma < \Sigma_{\max}$ since their size is N dependent. Thus, the system remains critical in the whole range $\Sigma < \Sigma_{\max}$ as long as plastic flow occurs, i.e., $\partial\Sigma/\partial\epsilon < \infty$. (ii) Avalanches become larger as $\Sigma \to \Sigma_{\max}$, as observed in Ref. [8], since $\partial\Sigma/\partial\epsilon \to 0$ at $\Sigma_{\max}$.

Further scaling relations can be derived for the statistical properties of transient avalanches for $\Sigma < \Sigma_{\max}$. We make the assumption that the distribution of avalanches $P(S)$ is homogeneous, i.e., $P(S) = S^{-\tau} f(S/S_c)$, where the cutoff size scales as $S_c \sim L^{d_f}$. Here, d_f is the fractal dimension of avalanches, L is the linear system size, and $N = L^d$, where d is the spatial dimension. From this distribution it is straightforward to compute the mean $\langle S\rangle \sim L^{d_f(2-\tau)}$. Comparing this with Eq. (1), we get

$$\tau = 2 - \frac{d}{d_f}\frac{\theta}{\theta+1}. \qquad (2)$$

A similar relation holds for stationary flow [13], although in the transient regime exponents appear to depend continuously on Σ.

Finally, we introduce an exponent γ, defined as $d\Sigma/d\epsilon \sim (\Sigma_{\max} - \Sigma)^{\gamma}$ for Σ close to $\Sigma_{\max}$. Equation (1) then implies the scaling relation

$$\langle S\rangle \sim (\Sigma_{\max} - \Sigma)^{-\gamma} N^{\theta/(\theta+1)}. \qquad (3)$$

These predictions are tested in Fig. 3. The inset of Fig. 3(a) shows that the mean avalanche size, as a function of $\Delta = [(\Sigma_{\max} - \Sigma)/\Sigma_{\max}]$, grows with the system size even far from failure. The entire solid phase is critical, as expected from Eq. (1). Note that to test this equation,

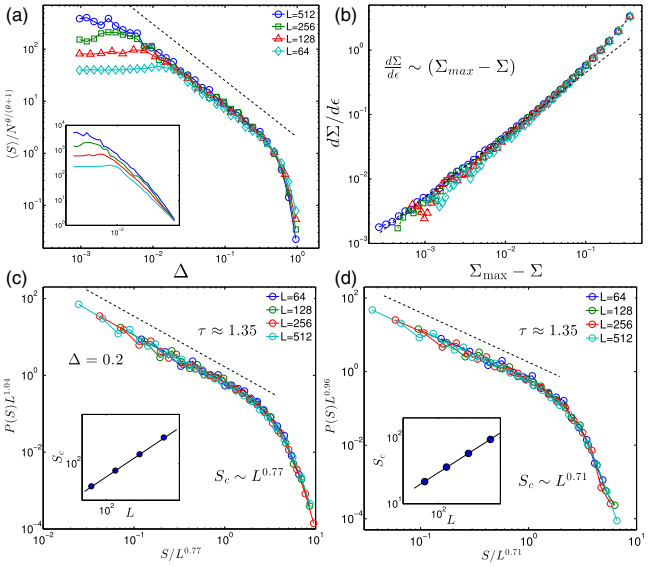

FIG. 3 (color online). (a) Collapse of the mean avalanche size as function of the proximity to failure $\Delta \equiv [(\Sigma_{\max} - \Sigma)/\Sigma_{\max}]$, using the value of $\theta(\Sigma)$ extracted from Fig. 2(b). The slope of the dotted line is -1.1. Here, $\Sigma_{\max}$ depends on the system size. The inset is the same quantity with no rescaling. (b) Local slope $d\Sigma/d\epsilon$ vs $\Sigma_{\max} - \Sigma$, supporting $\gamma \approx 1$, corresponding to $d\Sigma/d\epsilon \sim (\Sigma_{\max} - \Sigma)$ asymptotically. (c),(d) Collapse of the distribution of avalanche size at a specific stress value corresponding to $\Delta = 0.2$ for the stress-control case (c) and the strain-control case (d). We get $d_f \approx 0.77(0.71)$ in the stress- (strain-)control case, and $\tau \approx 1.35$ in both cases. All numerics are for $d = 2$.

one must consider the fact that $\theta = \theta(\Sigma)$. In this figure we use for $\theta(\Sigma)$ the third order polynomial fit of Fig. 2(b). Using these values for θ, a beautiful collapse is observed.

The presence of system sized avalanches far from threshold has to be distinguished from the divergence observed close to the yield stress, $\langle S\rangle \sim (\Sigma_{\max} - \Sigma)^{-\gamma}$ at fixed N, as implied by Eq. (3). Figure 3(a) is consistent with this relation and yields $\gamma \approx 1.1$. According to its definition, γ can also be directly measured from the local slope of stress-strain curves, as is done in Fig. 3(b), where $\gamma \approx 1$ is found, consistent with Fig. 3(a). $\gamma = 1$ means that the stress tends to $\Sigma_{\max}$ exponentially fast. As shown in the Supplemental Material [27], this appears to be valid also if the stress overshoots and $\Sigma_{\max} > \Sigma_c$.

In Figs. 3(c) and 3(d), we measure d_f at $\Delta = (\Sigma_{\max} - \Sigma)/\Sigma_{\max} = 0.2$, where $\theta \approx 0.33$, by collapsing the probability distribution of avalanche sizes, $P(S) \sim S^{-\tau} f(S/S_c)$, with $S_c \sim L^{d_f}$. We find $d_f \approx 0.77$ and $\tau \approx 1.35$ in the stress-control case. Again, these values perfectly agree with Eq. (2). This result holds also for the strain-control protocol, where we find scale-free avalanches with the same τ and a similar fractal dimension, $d_f \approx 0.71$.

Length scale.—To gather further evidence for the presence of a diverging length scale throughout the solid phase, we study the strain map generated by a single avalanche, and we consider the $M = (S-1)S/2$ distances $|\vec{R}_i - \vec{R}_j|$

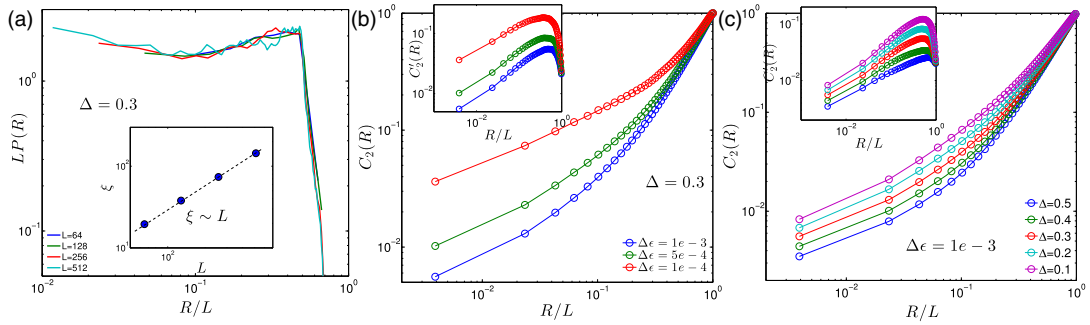

FIG. 4 (color online). (a) Distribution of avalanche extension $P(R)$ for the stress-control protocol at $\Delta = 0.3$. Collapse occur by rescaling distances with L, supporting the fact that $\xi = L$. (Inset) Direct measurement of ξ, defined as $\xi \sim \langle R \rangle$. (b) $C_2(R)$ at $\Delta = 0.3$ for different $\Delta\epsilon$'s, as indicated in the legend, suggesting a length scale that depends on $\Delta\epsilon$. (Inset) $C_2'(R)$ for which no such dependence appears. (c) $C_2(R)$ computed for $\Delta\epsilon = 10^{-3}$ and varying Δ as indicated in the legend, suggesting an increasing length scale as $\Delta \to 0$. (Inset) $C_2'(R)$ shows no such effect.

between all of the blocks involved in the avalanche. We compute the distribution of these distances and define $P(R)$ as the average of these distributions among avalanches occurring at the same stress value in different samples (we choose to weight each avalanche by M in this average). We focus on avalanches occurring at a finite distance from failure, with $\Delta \approx 0.3$. Assuming homogeneity, we expect $P(R) = (1/\xi^{\alpha}) g(R/\xi)$. In Fig. 4(a), we confirm such a form, specifically,

$$P(R) = \frac{1}{L} g\left(\frac{R}{L}\right). \tag{4}$$

We observe a similar scaling form in the strain-control simulation. These results confirm that $\xi \sim L$, as further supported by the observation that $\langle R \rangle \sim L$ (shown in the inset).

Our results are at odds with the conclusions of Ref. [10], which report an increasing length scale in a stress-control simulation of granular media. We now suggest that their data may in fact be consistent with our views. In Ref. [10], a length scale is extracted by considering the fluctuations of the strain field obtained during some strain interval $\Delta\epsilon$, for different stress values Σ. This is different *a priori* from our analysis above, which considers avalanches individually. To clarify this point, we perform an analysis closer to theirs, where finite intervals of strain are considered. We define a pair density function [34] $C_2(R)$ as the probability that two local plastic events among the $M \approx N\Delta\epsilon$ ones in this interval are at a distance smaller than R. Figure 4(b) shows $C_2(R)$ for $\Delta = 0.3$ and varying $\Delta\epsilon$'s, as indicated in the legend. At first sight, one may think that a length scale can be extracted from $C_2(R)$, but this length is $\Delta\epsilon$ dependent. We find that this dependence, however, can be cured by removing the effect of the mean strain in our definition of $C_2(R)$. We define $C_2'(R) = C_2(R) - C_2(L)R^2/L^2$, which is zero if the plastic events are homogeneous in space. As shown in the inset of Fig. 4(b), the characteristic length in $C_2'(R)$ does not depend on $\Delta\epsilon$. In Fig. 4(c) we show a similar analysis as the proximity to failure Δ is varied. From $C_2(R)$ it would appear that a length scale grows as $\Delta \to 0$. However, as shown in the inset, this is an artifact of this analysis, as $C_2'(R)$ shows a constant length scale of order L, consistent with our prediction $\xi = \infty$. Experimental measurements of the anisotropic part of the strain field also support that the correlation length is always large and weakly depends on Σ [9]. Our views could be further tested by performing a similar analysis in similar experimental [7–9] and numerical [10] data.

Conclusion.—Reference [20] argues that glassy systems whose elementary excitations display sufficiently long-range interactions (including electron glass, mean-field spin glasses, or spheres at random close packing) must display criticality for an entire range of fields or shear stress. This view has not yet been established experimentally. Our work supports that it holds in amorphous solids and granular materials, where it should be testable. Slowly sheared granular material experiments have revealed avalanches with power-law statistics, but currently these studies have been limited to stationary flow [35,36] (which, in addition, to miss the transient behavior, may lead to additional complexity for granular materials due to the emergence of isostaticity [37,38], a property, however, absent in the transient [39]). Note that for stresses far from $\Sigma_{\max}$, a large system may be required to test our views since one must have $\langle S \rangle \gg 1$ for Eq. (1) to hold. Our predictions may also apply in disordered crystals, where $\Sigma_{\max}$, however, is not well defined, presumably due to work hardening [40,41]. In Ref. [42], the authors observe numerically scale-free avalanches with $\langle S \rangle \sim N^{0.4}$ for a range of stresses. In our view that corresponds to $\theta \approx 0.67$, a prediction that could be tested by measuring how the characteristic interval of stress with no plasticity vanishes with N. Finally, a central question for the future is what governs the value of the exponent θ, which affects plasticity but also macroscopic rheological properties.

It is a pleasure to thank E. DeGiuli, E. Lerner, B. Metzger, M. Muller, J. Weiss, L. Yan, and S. Zapperi for the discussions related to this work. M. W. acknowledges support from NSF CBET Grant No. 1236378 and the MRSEC Program of the NSF, Grant No. DMR-0820341, for partial funding.

*jl4294@nyu.edu

[1] M. L. Manning, J. S. Langer, and J. M. Carlson, Phys. Rev. E **76**, 056106 (2007).
[2] B. Andreotti, Y. Forterre, and O. Pouliquen, *Granular Media: Between Fluid and Solid* (Cambridge University Press, Cambridge, England, 2013).
[3] E. A. Jagla, Phys. Rev. E **76**, 046119 (2007).
[4] T. Divoux, M. A. Fardin, S. Manneville, and S. Lerouge, Annu. Rev. Fluid Mech., doi:10.1146/annurev-fluid-122414-034416 (2015).
[5] R. L. Moorcroft and S. M. Fielding, Phys. Rev. Lett. **110**, 086001 (2013).
[6] D. A. Lockner and N. M. Beeler, Int. geophysics **81**, 505 (2002).
[7] A. Amon, V. B. Nguyen, A. Bruand, J. Crassous, and E. Clément, Phys. Rev. Lett. **108**, 135502 (2012).
[8] A. Le Bouil, A. Amon, J.-C. Sangleboeuf, H. Orain, P. Bésuelle, G. Viggiani, P. Chasle, and J. Crassous, Granular Matter **16**, 1 (2014).
[9] A. Le Bouil, A. Amon, S. McNamara, and J. Crassous, Phys. Rev. Lett. **112**, 246001 (2014).
[10] F. Gimbert, D. Amitrano, and J. Weiss, Europhys. Lett. **104**, 46001 (2013).
[11] A. Argon, Acta Metall. **27**, 47 (1979).
[12] O. Pouliquen, Phys. Rev. Lett. **93**, 248001 (2004).
[13] J. Lin, E. Lerner, A. Rosso, and M. Wyart, Proc. Natl. Acad. Sci. U.S.A. **111**, 14382 (2014).
[14] P. Olsson and S. Teitel, Phys. Rev. Lett. **99**, 178001 (2007).
[15] K. Martens, L. Bocquet, and J.-L. Barrat, Phys. Rev. Lett. **106**, 156001 (2011).
[16] G. Düring, E. Lerner, and M. Wyart, Phys. Rev. E **89**, 022305 (2014).
[17] K. M. Salerno, C. E. Maloney, and M. O. Robbins, Phys. Rev. Lett. **109**, 105703 (2012).
[18] A. Lemaître and C. Caroli, Phys. Rev. Lett. **103**, 065501 (2009).
[19] D. S. Fisher, Phys. Rep. **301**, 113 (1998).
[20] M. Müller and M. Wyart, Annu. Rev. Condens. Matter Phys. **6**, 177 (2015).
[21] J. Lin, A. Saade, E. Lerner, A. Rosso, and M. Wyart, Europhys. Lett. **105**, 26003 (2014).
[22] G. Picard, A. Ajdari, F. Lequeux, and L. Bocquet, Phys. Rev. E **71**, 010501 (2005).
[23] J.-C. Baret, D. Vandembroucq, and S. Roux, Phys. Rev. Lett. **89**, 195506 (2002).
[24] P. Hébraud and F. Lequeux, Phys. Rev. Lett. **81**, 2934 (1998).
[25] G. Picard, A. Ajdari, F. Lequeux, and L. Bocquet, Eur. Phys. J. E **15**, 371 (2004).
[26] D. Vandembroucq and S. Roux, Phys. Rev. B **84**, 134210 (2011).
[27] See Supplemental Material at http://link.aps.org/supplemental/10.1103/PhysRevLett.115.168001 for the discussion on the initial conditions and finite size effects of $P(x)$.
[28] Y. Shi, M. B. Katz, H. Li, and M. L. Falk, Phys. Rev. Lett. **98**, 185505 (2007).
[29] R. L. Moorcroft, M. E. Cates, and S. M. Fielding, Phys. Rev. Lett. **106**, 055502 (2011).
[30] S. M. Fielding, Rep. Prog. Phys. **77**, 102601 (2014).
[31] A. Lemaître and C. Caroli, arXiv:0705.3122.
[32] S. Karmakar, E. Lerner, and I. Procaccia, Phys. Rev. E **82**, 055103 (2010).
[33] K. M. Salerno and M. O. Robbins, Phys. Rev. E **88**, 062206 (2013).
[34] L. Girard, D. Amitrano, and J. Weiss, J. Stat. Mech. (2010) P01013.
[35] N. W. Hayman, L. Ducloué, K. L. Foco, and K. E. Daniels, Pure Appl. Geophys. **168**, 2239 (2011).
[36] M. Bretz, R. Zaretzki, S. B. Field, N. Mitarai, and F. Nori, Europhys. Lett. **74**, 1116 (2006).
[37] E. DeGiuli, G. Düring, E. Lerner, and M. Wyart, Phys. Rev. E **91**, 062206 (2015).
[38] E. Lerner, G. Düring, and M. Wyart, Proc. Natl. Acad. Sci. U.S.A. **109**, 4798 (2012).
[39] N. P. Kruyt, C.R. Mec. **338**, 596 (2010).
[40] M.-C. Miguel, A. Vespignani, S. Zapperi, J. Weiss, and J.-R. Grasso, Nature (London) **410**, 667 (2001).
[41] F. F. Csikor, C. Motz, D. Weygand, M. Zaiser, and S. Zapperi, Science **318**, 251 (2007).
[42] P. D. Ispánovity, L. Laurson, M. Zaiser, I. Groma, S. Zapperi, and M. J. Alava, Phys. Rev. Lett. **112**, 235501 (2014).